Virtual reconstruction of the painting process and original colors of a color-changed Northern Wei Dynasty mural in Cave 254 of the Mogao Grottoes

Chai Bolong
Northwestern University School of Cultural Heritage
Yu Zongren
Dunhuang Academy
Sun Manli
Northwestern University School of Cultural Heritage
Shan Zhongwei
Dunhuang Academy
Zhao Jinli
Dunhuang Academy
Shui Biwen
Dunhuang Academy
Wang Zhuo
Dunhuang Academy
Yin Yaopeng
Dunhuang Academy
Su Bomin (SuBomin_dha@126.com)
Dunhuang Academy

Research Article

Keywords: Virtual reconstruction, multispectral imaging, pigment analysis, mechanisms of pigment color changes

Posted Date: May 18th, 2022

DOI: https://doi.org/10.21203/rs.3.rs-1640179/v1

Abstract

The Northern Wei Dynasty (386–534 CE) murals of Cave 254 in the Mogao Grottoes, China, have been extensively affected by pigment color changes and fading. These issues severely hinder efforts to correctly understand the value and painting process of murals from this historic period. The virtual reconstruction of faded murals could help researchers gain an understanding of their pigment chemistry and painting processes in a virtual environment and provide a visual reference for conservation and art studies. However, simple virtual reconstructions may not be accurate owing to deficiencies in our understanding of the color-changed pigments and fading of image lines. In this study, a minimally invasive approach was used to elucidate the details and pigment distributions of a faded mural. Technical photography was performed to obtain infrared-reflected false color, ultraviolet-reflected false color, and ultraviolet luminescence images of the mural. Noninvasive and minimally invasive analyses were then performed on localized parts of each color-area to identify their pigments and paint stratigraphy and construct a hue–saturation–brightness color palette for these pigments. Finally, the pigment analysis results were combined with multispectral image features to determine the pigment distributions of the mural, which were then used to virtually reconstruct the original color and appearance of the faded mural under ideal conditions. This study is the first to use a virtual reconstruction based on objective analyses to simulate the original color, painting processes, and pigment stratigraphy of a mural from the Northern Wei Dynasty. A preliminary discussion of the relationship between the painting processes of the mural and color changes in its pigments was also performed. The findings of this study will provide new perspectives for the study of Northern Wei Dynasty murals.

Introduction

The Mogao Grottoes is located 25 km southeast of Dunhuang City, Gansu Province, China. It is a cave system containing some 735 caves, 492 of which contain polychromatic sculptures and murals. The oldest caves in this system were constructed in 366 CE, during the Former Qin Dynasty. The construction of these caves continued for over 1600 years, until the end of the Yuan Dynasty (1271–1368 CE). As a whole, the Mogao Grottoes contain 45,000 m^2 of murals and over 2000 polychromatic sculptures, which contain information on the livelihoods, cultures, religions, and arts of 10 different dynasties, thereby rendering it one of the most important grottos in the world. In 1987, the United Nations Educational, Scientific, and Cultural Organization (UNESCO) inducted the Mogao Grottoes into the UNESCO World Heritage List. The murals in Cave 254, which was dug during the Northern Wei Dynasty, are representative of Mogao grotto art from this period. The Buddhist mural (i.e., pictures representing a story from Buddhist scripture) on the southern wall of this cave is “Prince Sattva Sacrifices Himself to the Starving Tigress” (hereafter referred to as “Prince Sattva”), one of best-known stories in Buddhist mythology. Because this mural combines Indian and West Asian Buddhism with the traditional Chinese style, it is immensely valuable for studies on the propagation of Buddhist art in China and its integration with local Chinese art. Furthermore, detailed studies on this mural could improve methods to preserve and repair murals from this period. The Prince Sattva mural measures 168 cm wide and 150 cm tall, and it narrates a story from

a past life of the Buddha using a series of pictures within a rectangular space. Each picture represents an event that occurred at a different time and place. This approach overcomes the limitations of 2D art in its ability to describe the passage of time, and the mural is a classic example of the narrative illustrations that emerged after the Han Dynasty (202 BCE–220 CE). The story told by this mural consists of five scenes: (1) Prince Sattva vows to save the tigress; (2) the prince pierces his neck and dives from the cliff; (3) the tigress feeds herself on Sattva's body; (4) Sattva's family mourns his death; and (5) Apsarases (a celestial being in Indian mythology) floats around a pagoda holding Sattva's bones (Fig. 1). Owing to the importance of this particular mural in the history of the Mogao murals, many artists and conservationists have shown great interest in the pigments, colors, and painting processes used in this mural, as well as its artistic value [1–4]. Many have attempted to reimagine the original color and appearance of this mural, and, to this end, a variety of methods have been used to reconstruct the mural.

In the past, the main purpose of mural reconstruction research was to study fine arts and obtain a virtual presentation of restoration effects. Research in this field usually takes on the forms of art replication and virtual reconstruction [5]. Art replication is performed by experienced artists, and it is a subjective process based on comparisons with well-preserved murals that are contemporary to the degraded, to-be-replicated mural. An example of art replication being used to reconstruct a mural is the "Donor portrait of Lady Wang from Taiyuan in worship" from Cave 130, which was replicated by Duan Wenjie [6]. Virtual reconstruction, an approach that is currently in vogue, refers to the use of computational image processing algorithms, such as image segmentation, texture synthesis, machine learning and neural networks, to digitally reconstruct the color and details of an artistic product [7–12]. These methods could inform and pave the way for future attempts to recreate the original appearance of ancient murals. Unfortunately, such techniques may be inapplicable to murals with changed colors owing to gaps in our knowledge on the faded image and its color-changed pigments. The accuracy of digital replicas or reconstructions based on machine learning can also be affected by the conditions of the working space, the quality of the image pixels, and the accuracy of the pigment-color analysis. Furthermore, machine learning methods require massive amounts of data, and constructing the large number of sample models required by these methods within a short time is difficult. This limitation could ultimately reduce the accuracy of color classification and reconstruction by machine learning methods.

The Mogao murals are well known to have a base layer consisting of coarse (sand and wheat-straw) and fine (sand + bast and leaf fiber) soils, which are covered by preparatory and pigment layers. Repeated studies by scholars and research institutes in China and beyond have confirmed that the colors used in the Mogao murals primarily consist of red, blue, green, white, and black, which come from over 20 natural mineral pigments. Some of the murals even use organic dyes, such as indigo, lac, and madder [13–18]. Environmental factors and the complexity of the pigments and painting techniques render these murals susceptible to pigment degradation, which leads to color changes. For instance, pigments containing Hg, Pb, and As are easily degraded by photochemical reactions, air pollution, and microbial action or other complex chemical reactions, which could change their color and appearance [19–24]. Organic pigments are also susceptible to photochemical or microbial degradation [25]; thus, assessing whether organic pigments were applied to a mural using visible light alone is difficult. The Mogao murals are extensively

affected by these chemical changes, and accurately ascertaining the original colors of the faded murals and objectively performing virtual reconstructions of these murals are challenging.

In this work, we created a digital representation of the Prince Sattva mural based on an extensive investigation and analysis of its color pigments. Compared with previous forms of mural reconstruction, digital reconstruction (for mural preservation and artistic research) enables the final visualization of extensive studies and provides a deeper understanding of the simulation and analyses of the pigment usage rules and painting procedures of Northern Wei Dynasty murals. The results of our efforts to restore the colors of the original frescoes and faded details of the images can be used as a visual aid to support pigment analysis and process understanding. As the pigment analysis method used in this work is undoubtedly the pillar technology of cultural relic protection, our comprehensive analysis results could serve as an important basis for improving the objectivity and feasibility of the virtual reconstruction of discolored and faded murals. Moreover, our findings present a new perspective for the analysis and display of murals in the Mogao Grottoes.

Methodology And Equipment

Methodology

The processes of virtual reconstruction can be broadly divided into two parts: preliminary investigation and digital painting restoration. The first part involves the extraction of information from the faded image and the study of pigment types, both of which are necessary for objective and realistic virtual reconstructions. The study of faded and color-changed pigments is the primary focus and challenge of this work.

First, ultraviolet-induced visible luminescence (UVL) and infrared-reflected (IRR) images were used to detect organic dyes and degraded details that are invisible to the naked eye. Infrared-reflected false color (IRRFC) and UV-reflected false color (UVRFC) images were then used to determine the areas that were painted with each type of pigment as pigments of the same type will have similar false colors in IRRFC and UVRFC images. However, as the mural contains complex mixtures and layers of color and is affected by color changes, identifying pigments based on the multispectral images of standard pigment samples is not a straightforward task. In other words, the IRRFC and UVRFC characteristics of the mural may not perfectly match those of the multispectral reference. Nonetheless, pigments of the same type will exhibit similarities in certain spectral bands, so IRRFC and UVRFC images could be used to preliminarily determine the distribution of unidentified pigments in the mural. The exact identification of pigments and color-changed compounds can only be achieved using noninvasive and/or minimally invasive analytical methods when conditions permit.

Next, instruments were used to elucidate the relationship between pigment type and color in each color-area of the mural and assess the effects of paint layering on surface color. As minimizing damage to the mural is necessary, only microscopic amounts of samples were obtained from damaged parts of the

pigment layer. Each sample was then analyzed using a variety of instruments. Finally, the instrumental analysis results were combined with the IRRFC and UVRFC images to identify the distribution of each pigment in the mural.

Based on the results of the aforementioned pigment analysis, the hue–saturation–brightness (HSB) values of the pigments used in the mural were extracted from their corresponding visible-reflected (VISR) images in the multispectral reference. These HSB values were then used to construct a digital color palette. Finally, the mural was virtually reconstructed by drawing its lines according to the details revealed by its multispectral images and then coloring the mural according to the pigment distribution data.

Equipment

Multispectral imaging equipment

A modified Nikon D7000 camera with a maximum resolution of 4928 px × 3264 px (16.2 MP) was used for multispectral imaging (UV-VIS-IR). The spectral response of this camera's sensor was expanded to approximately 300–1,000 nm by removing its built-in IR filter [26–28]. A 35 mm f2.8 DX lens was installed on the camera, and the spectral bandwidth of the camera was limited using various filters. A pair of Godox AD360 halogen flashes [360 W, 5,600 ± 200 K, 80 (M ISO 100), 1/10,000–1/300 S] were used as light sources. These flashes were modified by replacing their plastic filters with a variety of filters depending on the desired spectral bandwidth. The use of bandpass filters on the light source and receiver (camera lens) has been proven to be a reliable method to obtain multispectral images because it eliminates the need for different light sources for each spectral band and reduces the need for total darkness during the acquisition of multispectral images (especially photoluminescence images). Professor Giovanni Verri has contributed tremendously to the development of this approach [29]. The bandwidths of the filter sets used in this study are shown in Table 1.

Table 1
Incoming and outgoing filter sets used for reflectance and luminescence imaging

Method	Flash filters (77 mm)	Excitation band range	Lens filters (52 mm)	Emission band range
VISR	Plastic diffuser	185–2,000 nm	IDAS (360–700 nm) + KV418 (cut-on above 400 nm)	400–700 nm
IRR	——	185–2,000 nm	Schott RG715/830/1,000 (cut-on above 715/830/1000 nm)	715–1000 nm
UVR	XNiteCC1 (330–700 nm) +XNite330C (200–400 nm)	330–400 nm	XNiteCC1 (330–700 nm) + XNite330C Short pass (200–400 nm)	330–400 nm
UVL	XNiteCC1 (330–700 nm) + XNite330C (200–400 nm)	330–400 nm	IDAS (360–700 nm) + KV418 (cut-on above 400 nm)	400–700 nm

Note. VISR = visible light reflectance; IRR = infrared reflectance; UVR = ultraviolet reflectance; UVL = ultraviolet-induced luminous. Filter source: https://maxmax.com/. The plastic diffuser does not block ultraviolet light.

Besides the camera, light source, and filters, the X-rite Color Checker and Spectralon® reflectance standards are also important accessories for multispectral imaging as They are used for correction of color and diffuse reflection spectra. All multispectral images were taken in manual mode. The parameters of the VISR and IRR images were F8, 1/200 S, and ISO: 100. The parameters of the UVR images were F2.8, 1/200 S, and ISO: 100. The parameters of the UVL images were F2.8, 1/200 S, and ISO: 400. The two light sources were oriented symmetrically about the focal axis of the camera at an angle of 45°, and the power of the flashes was adjusted according to the straight-line distance between the lens and mural. Post-processing of the spectral images and generation of false color images were performed using Photoshop and Nip2 and BM-workspace [30–35]. The postprocessing procedures, workflows, and data requirements are detailed in Refs. [36, 37].

Multispectral references

In this study, multispectral references refer to the multispectral image files used for pigment identification. These files were obtained by taking multispectral images of pigments mixed with a special adhesive in the 360–1,000 nm range with the same photographic parameters and postprocessing procedures used to collect the multispectral images of the research subject. Comparison of the spectral reflectances and luminescent properties enabled the use of these files for identifying monolayered pigments in some research subjects. This approach has been extensively studied and characterized by a number of

scholars [38, 39]. However, because the pigment samples were obtained from a variety of modern producers and not the mural itself, X-ray diffraction (XRD) analysis must first be performed to confirm that the pigment samples are usable for this purpose. As we had previously performed an experimental study on multispectral references for the pigments used in Mogao murals (Supplementary Materials 2 and 3), we refer the reader to Ref. [40] for a detailed description of the process through which these references were obtained. In this study, the reference files were also used to assess the chroma and hue of the pigments prior to their color change by extracting the HSB values of the target pigment from the VISR image in its multispectral reference files. These HSB values were then used to create a digital color palette, which was used to color the virtually reconstructed mural.

Portable X-ray fluorescence (pXRF) analyzer

The pXRF instrument used in this study was a Thermo Fisher Scientific (USA) Niton XL3t 800, which employs a Ag target as its excitation source. The parameters of the pXRF were as follows: tube voltage: 6–50 kV, tube current: 0–200 μA, power: ≤2 W, detector: Si-PIN (Si semiconductor detector), resolution: <190 eV, detection time: 60 s, diameter of analyzed area: 8 mm.

X-ray diffractometer

A DMAX/2500 X-ray diffractometer was used to perform XRD analysis. The measurements were performed in continuous-scan mode over the 2θ range of 5°–70° with a tube voltage of 40 kV and tube current of 100 mA. Mixed layers from the pigment layer were used as samples, and each sample weighed approximately 0.2 g.

Scanning electron microscope and energy dispersive X-ray (SEM-EDS) spectroscope

SEM-EDS spectroscopy was performed using a JSM-6610LV scanning electron microscope (JEOL Ltd., Japan). The analysis was performed with an acceleration voltage of 25 kV, resolution of 5.0 nm, and magnification of 5×–30,000× in vacuum mode. A polarized microscope was used to observe 0.2 mg pigment samples and select cross sections of interest. The samples were embedded in epoxy, polished, platinized, and then placed in the sample chamber of the SEM for cross-sectional analysis.

Liquid chromatograph–mass spectrometer (LC/MS)

LC/MS was performed using a Thermo Scientific Q Exactive hybrid quadrupole-Orbitrap high-resolution tandem mass spectrometer in heated electrospray mode. The LC parameters were as follows: spray voltage: 3.5 KV, sheath gas pressure: 45 arb; auxiliary gas pressure: 10 arb, capillary temperature: 275°C, heater temperature: 450°C. The mass spectrometer was operated in full MS-ddMS^2 mode, and the mass resolution was set to 70,000 FWHM for full-scan MS (first stage) and 17,500 FWHM for dd-M^2 (second stage). Stepped normalized collision energies of 20%, 40%, and 80% were used. The samples were dissolved in 200 mL of methanol and centrifugated. The supernatant was used for LC/MS analysis.

Portable digital microscope (pDM)

A VH-Z20R (20×–200×) lens and Keyence VHX-600E digital microscope (with a built-in illuminator) were used for visible-light microscopy.

Raman spectrometer

A LabRAM XploRA (Horiba, France) mini laser Raman spectrometer (MLRS) was used for Raman spectroscopy. This instrument includes a high-stability research-grade microscope with reflective and transmissive Köhler illumination and is equipped with 10×, 100×, and long working distance 50× objectives. The instrument also includes high-stability 532 and 785 nm fixed lasers (and their filters), as well as a computer-controlled multilevel laser attenuator. The microscope is fully confocal; when equipped with a 100× objective, its spatial resolution is < 1 μm in the XY direction and < 2 μm in the Z direction. The system is equipped with four gratings (2,400 gr/mm, 1,800 gr/mm, 1,200 gr/mm, and 600 gr/mm) and has a spectral resolution of $\leq 2\ cm^{-1}$. Its spectral repeatability is greater than $\pm 0.2\ cm^{-1}$. Two excitation wavelengths (532 and 785 nm) were simultaneously used in this experiment. The 532 nm excitation has a higher laser power but also a very strong fluorescence background. By comparison, the 785 nm excitation has a weaker laser background. The range of experimentally measured Raman frequency shifts was 100–3,000 cm^{-1}.

Digital restoration tools

Digital restoration was performed using Adobe Photoshop, the Procreate raster graphics editor app, and a Wacom Intuos Pro PTH660 tablet.

Results And Discussion

Investigation of image details

Multispectral images can reveal many details that are invisible to the naked eye. In Scene 2, the 830 nm IRR image revealed traces of a mesh-like pattern on the prince's hair bun (Fig. 2-a). These traces appear to the degraded remains of a crown, which is commonly used in ancient China as a decoration for hair buns. Crowns are uncommon in paintings on the same theme in the Mogao Grottoes. The UVL images revealed bloody scenes that are invisible to the naked eye, such as blood spurting out of the prince's throat when he committed suicide in Scene 2 (Fig. 2-b) and coming out of the tigers' mouths when they bit into the prince's body in Scene 3 (Fig. 2-c). The circular, regularly arranged luminescent dots that appear in Scenes 2 (the prince's suicide) and 5 (around the pagoda) also caught our attention. As these dots appeared in the suicide and funeral scenes, they may be deduced to be Buddhist Śarīra, which represent the attainment of perfect moral conduct, inner peace, and wisdom; in other words, they are signs of the Bodhisattva's enlightenment (Fig. 2-d).

The VISR image also revealed traces of an artist making changes to the mural, which are strengthened in the IRR image. As can be seen in the VISR images, Scene 1 shows two modifications: the raised hand of the prince was moved rightward (Fig. 2-e) and the finger of the prince's younger brother (to his right) was

changed from curled to outstretched (Fig. 2-g). In the IRR images, the tail of a tiger cub in Scene 3 was changed from straight to sloping downward, thereby rendering the posture of the tiger cub more balanced (Fig. 2-f). In Scene 4, the left side of the Bodhisattva's robe is faintly outlined. In the final painting, however, his body was made to curve and move rightward, giving him a more dynamic and realistic appearance (Fig. 2-h).

Pigment analysis

Overall, the VISR (Fig. 3), IRRFC (Fig. 4), UVFRC (Fig. 5), and UVL (Fig. 6) images clearly revealed the different color-areas of the mural. The VISR images showed that the mural currently has 10 color systems, including blue, bean green, ivory white, pure white, light red, charcoal gray, black–brown, maroon, deep red, and red–brown. The UVFRC images distinguished areas that were painted blue and bean green. The IRRFC images showed the boundaries of multiple color-areas, and the UVL images illustrated the distribution of pigments with similar luminescent properties. The full-scene multispectral images depicting details of the mural are shown in Supplementary Material 1. According to the results of our multiband imaging surveys, the mural appears to have been painted using a mixing-and-layering process. Thus, identifying pigments using the multispectral images alone is difficult. Therefore, an instrumental analysis was performed on 10 representative color-areas of the mural (Table 2). In Figs. 3–6, the sampling points selected for instrumental analysis and multispectral imaging of the localized details of the mural are as follows: (a) [1] blue, [2] bean green; (b) [3] ivory white, [4] pure white; (c) [5] light red; (d) [6] charcoal gray, [7] black–brown, [8] maroon; (e) [9] deep red, [10] red–brown. A summary of the results of this analysis is shown in Table 3.

Table 2. Color description of mural pigments in the multispectral images

Test No.	VISR < 400–700 nm <	H S B	IRRFC < 830 nm	H S B	UVRFC < 365–400 nm <	H S B	UVL Excitation: 365 Emission: 400–700 nm	H S B
1	Blue	218 23 43	Pink	346 17 48	Olive green	102 26 45	——	240 62 3
2	Bean green	185 16 60	Blue	213 26 53	Tea green	62 43 62	——	225 44 4
3	Ivory white	60 10 75	Milky white	51 7 77	Off white	42 35 74	Deep iron blue	192 29 14
4	White	41 10 72	Milky white	49 6 77	Off white	38 27 72	Deep iron blue	150 16 15
5	Light red	18 47 64	Pale lemon yellow	48 42 72	Dark brown	300 16 31	Salmon	16 48 66
6	Charcoal grey	36 6 35	Emerald black	168 54 36	Charcoal grey	266 13 43	Blue green	12 3 17 42
7	Black brown	11 33 26	Olive brown	47 40 42	Blue black	227 47 42	——	225 44 4
8	Maroon	16 46 44	Jade green	87 35 42	Charcoal grey	195 4 44	Salmon	23 58 57
9	Deep red	355 71 25	orange brown	38 63 36	Olive black	246 56 20	Salmon	20 55 42
10	Red brown	12 51 39	Black yellow green	59 52 50	Clay	16 24 31	——	0 14 3

Note: This table denotes the false colors in the UVRFC and IRRFC images representing the current VISR colors of the mural. The HSB (H: hue, S: saturation B: brightness) values of each color are also indicated.

Table 3
Summary of the main color-area findings

Analysis location	Current color	Global XRF[e]++	XRD analysis of the mixture [c]++	LC/ MS	Pigment layer SEM-EDS[e]++	Pigment layer MLRS [c]++	Main pigment and stratigraphic sequence+++
NO. 1	Blue	Cu, Fe, As	Quartz, Azurite, Atacamite, Dioptase, Dickite, Laumontite	——	1: Cl, Cu, O, Si, Al, K 2: Cl, Ca, O, Cu, Si, Fe, Mg, Al, S, K	——	1. Azurite, 2. Atacamite
NO. 2	Bean green	Cu, Fe, As	Quartz, Azurite, Atacamite, Dioptase, Dolomite, Laumontite, Albite, Gypsum	——	——	——	1. Atacamite, 2. Azurite, 3. Gypsum
NO. 3	Ivory white	Fe, Ca	Quartz, Gypsum, Talc, Lizardite, Hemihydrate, Gypsum, Clinochlore-1MIIb	——	——	——	1. Talc, Gypsum
NO. 4	Pure White	Pb, Fe	Quartz, Gypsum, Red lead, Clinochlore, PbO, Leucite, Felsobanyaite	——	——	——	1. Gypsum, 2. Red lead, litharge
NO. 5	Light red	Fe, Pb, Ca, As	Quartz, PbO, Clinochlore, Gypsum, Felsobanyaite	Lac dye	1: Cl, Ca, Si, O, Fe, Na, Mg,Al K, C	——	1. Lac dye, 2. Gypsum, 3. Litharge
NO. 6	Charcoal grey	As, Hg, Fe, Ca	Quartz, Azurite, Gypsum, Dickite, Arsenolite	——	2: Cl, Ca, Si, Hg, As, Al, Mg,O, C, K, Fe 3: Cl, Ca, Si, Mg,As, Al, O, Fe, S, C	——	1. Realgar, 2. Gypsum

Note: Conclusive results (+++), supportive results (++). c: Primary pigment-related components. e: Pigment-related elements. (-): No relevant testing performed.

Analysis location	Current color	Global XRF[e]++	XRD analysis of the mixture [c]++	LC/MS	Pigment layer SEM-EDS[e]++	Pigment layer MLRS [c]++	Main pigment and stratigraphic sequence+++
NO. 7	Black brown	Fe, As, Ca, Pb, Hg	Quartz, Carminite, Clinochlore, Illite, Cinnabar, Calcite	——	2: Ca, Fe, O, Si, Al, As, Mg, K, S	——	1. Cinnabar, 2. Realgar, 3. Calcite
NO. 8	Maroon	Fe, Pb, As, Ca	Quartz, Carminite, Clinochlore, Anorthoclase, Illite, Calcite	——	2: Cl, Ca, Si, Mg, O, Al, Fe, C 3: Cl, Ca, Si, As, Mg, O, Pb, Al 4: Cl, Ca, Si, Mg, O, Fe, Al, C, S	—— 3.$PbCl_2$ 4.Pb_3O_4	1. Lac dye, 2. Calcite, 3. Realgar + Cotunnite
NO. 9	Deep red	Pb, Hg, As, Fe	Quartz, PbO, Calcite	——	2: Hg, Si, O, Al, As, C 3: Pb, O, C	——	1. Lac, 2. Cinnabar, 3. Litharge, 4. Calcite
NO. 10	Red brown	Pb, Fe	Red lead, Massicot	——	——	——	1. Red lead, 2. Litharge

Note: Conclusive results (+++), supportive results (++). c: Primary pigment-related components. e: Pigment-related elements. (-): No relevant testing performed.

Blue and bean-green areas

The colors blue and bean-green cover wide parts of the mural, and their boundaries are difficult to distinguish in the VISR image (Fig. 3-a[1, 2]). However, because the pigments used in these colors show different reflectances in the IR band, clearly delineating their boundaries in the IRRFC image is possible. The blue and bean-green pigments in the IRRFC image are pink and blue, respectively, (Fig. 4-a[1, 2]). Although the delineation of pigment boundaries can be achieved, the direct identification of their origin using multispectral false color images alone is not yet possible. The pDM observations indicate some layering and mixing between the blue and bean-green pigments (Figs. 7-a[1] and 7-b[2]). The pXRF results show that these two pigment areas contain high concentrations of Cu, followed by Fe and Ca (Fig. 7-b[1, 2]). Microsamples of these pigments were used to prepare epoxy-embedded cross sections. In the cross-sectional microscopic observations, mixing and layering could be observed between the blue and bean-green pigment particles, with the blue (layer 1) pigments lying on top of the bean-green (layer 2)

pigments. The total thickness of these layers is 34.4 μm. A white 28.7 μm-thick layer (layer 3) is also present below the blue layer, the white pigment particles of which are sparsely mixed with the base layer (Fig. 8-a[1]). These three pigments make up a 34.0–55.0 μm-thick mixed-pigmented layer (Fig. 8-b[2]). Based on the SEM-EDS analysis, the blue layer (layer 1) contains Cl, Cu, O, Si, Al, and K and the bean-green layer (layer 2) contains Cl, Ca, O, Cu, Si, Fe, Mg, Al, S, and K (Fig. 9-a). Based on the XRD analyses of microsamples collected from the same locations, both sets of samples contain quartz [SiO_2], azurite [$Cu(CO_3)_2(OH)_2$], atacamite [$Cu_2Cl(OH)_3$], dioptase [$Cu_6Si_6O_{18}·6H_2O$], and laumontite [$Ca(AlSi_2O_6)_2·4H_2O$] phases. The bean-green samples also contain albite [$NaAlSi_3O_8$] and gypsum [$CaSO_4·2H_2O$] phases (Figs. <link rid="fig6">10</link>-a and 10-b).

By analyzing the aforementioned results, we can conclude that the blue and bean-green parts of the mural correspond to azurite and atacamite, respectively. The preparatory layer of these pigments is a white clay that predominantly consists of gypsum.

White areas

The white pigment is mainly located in the pagoda in Scene 5 and highlights, such as the clothes and skin of human characters (Fig. 3-b[3, 4]). Because the reflectances of these white pigments are very similar, delineating their boundaries and determining their origin using multispectral images is quite difficult. In the IRRFC images, all of the white areas are milky white (Fig. 4-b[3, 4]); in the UVRFC images, they are all off-white (Fig. 5-b[3, 4]). In the 365 nm-excited UVL images, the white areas show a dim metallic-blue luminescence (Fig. 6-b[3, 4]). Based on pDM observations, the white parts of the mural have two different shades; the larger areas are painted in ivory white (Fig. 7-a[3]) while the local highlights are painted in pure white (Fig. 7-a[4]). The pDM observations also indicate that the ivory-white and pure-white parts have maroon and red–brown preparatory layers, respectively. Based on pXRF analysis, the ivory-white parts contain high concentrations of Fe, as well as Ca, while the pure-white parts contain high concentrations of Pb, as well as Fe (Figs. 7-b[3] and 7-b[4]). As the stratigraphy of the ivory-white pigments is relatively simple, we only prepared an epoxy-embedded cross section of the pure-white pigment. This cross section showed a pure-white pigment layer measuring approximately 25.0 μm in thickness lying on top of a red–brown preparatory layer (Fig. 8-c[4]). Based on XRD analysis, the ivory-white areas are painted with a clay-mineral pigment predominantly consisting of talcum [$Mg_3Si_4O_{10}(OH)_2$] and containing quartz [SiO_2], gypsum [$CaSO_4·2H_2O$], lizardite [$(Mg_3Si_2O_5(OH)_4$], hemihydrate gypsum [$CaSO_40.5H_2O$], and clinochlore [$Mg_5Al(AlSi_3)O_{10}(OH)_8$] (Fig. 10-c). The pure-white areas are painted with a clay-mineral pigment that mainly consists of gypsum [$CaSO_4·2H_2O$], as well as albite [$NaAlSi_3O_8$], leucite [$KAlSi_2O_6$], and felsobanyaite [$Al_4(SO_4)(OH)_{10}·4H_2O$] (Fig. 10-d). The pure-white sample also shows intense red lead [Pb_3O_4], litharge [PbO], and arsenolite [As_4O_6] phases [41]. These components most likely originated from the red–brown pigment and base layer, which serve as the mural's background and preparatory layer. Therefore, a pigment layer consisting of a mixture of red lead and litharge should be found below the pure-white pigment. This layer is actually the background color of the mural, and the pure-white pigment is painted directly over it. The red–brown background will be further described in detail in a later section.

Light-red areas

The light-red pigment appears in Scenes 1–3 on the clothes of human characters and some mountains (Fig. 3-c[5]). The light-red pigment is light lemon yellow in the IRRFC image (Fig. 4-c[5]) and emits an intense salmon luminescence in the 365 nm-excited UVL image (Fig. 6-c[5]). This finding indicates that an organic paint may be present in the light-red parts of the mural. The deep-red pigments and some maroon pigments (which will be discussed in later sections) also exhibit this type of luminescence. pDM observations of a damaged part of the mural show bright-red, white, light-red, and yellow pigments, as well as an earthen base layer (Fig. 7-a[5]). The pXRF analysis shows that this region has high concentrations of Fe, Pb, and Ca (Fig. 7-b[5]). In the cross-sectional pigment sample, the light-red area consists of a 5.7 μm-thick red pigment layer that covers the white and yellow pigment layers(Fig. 8-d[5]). The SEM-EDS analysis indicates that the bright-red layer contains Cl, Ca, Si, O, Fe, Na, Mg, Al, K, and C (Fig. 9-b). The XRD analysis shows that the light-red parts of the mural contain quartz [SiO_2], litharge [PbO], clinochlore [$Mg_5Al(AlSi_3)O_{10}(OH)_8$], gypsum [$CaSO_4{\cdot}2H_2O$], and felsobanyaite [$Al_4(SO_4)(OH)_{10}{\cdot}4H_2O$] phases (Fig. 10-e), with litharge and felsobanyaite possessing the most intense diffraction peaks. Therefore, the yellow pigment in the pigment mixture is mainly litharge, and the white pigment is a white gypsum-dominated clay-mineral mixture.

LC-MS analysis was performed on the light- and deep-red pigments producing salmon luminescence (Fig. 11-[a–e]). The retention time of component 1 was 1.22 min, and its pseudo-molecular ion $[M\text{-}H]^-$ peak at the first-stage MS level was observed at m/z 295.11851, which fits the molecular formula $C_{15}H_{20}O_6$. At the second-stage MS level, characteristic fragment ions were observed at m/z 251.12863, 249.11327, 177.12842, and 121.06597. This compound was thus identified as shellolic acid.

The retention time of component 2 was 2.25 min, and its pseudo-molecular ion $[M\text{-}H]^-$ peak at the first-stage MS level was observed at m/z 293.10265, which fits the molecular formula $C_{15}H_{18}O_6$. At the second-stage MS level, characteristic fragment ions were observed at m/z 249.11295, 205.12337, 109.06588, and 83.05025. This compound was identified as oxidized shellolic acid.

The retention time of component 3 was 2.99 min, and its pseudo molecular ion $[M\text{-}H]^-$ peak at the first-stage MS level was observed at m/z 279.12350, which fits the molecular formula $C_{15}H_{20}O_5$. The characteristic fragment ions of this component at the second-stage MS level were observed at m/z 261.11285, 235.13353, 217.12303, 147.04492, and 119.05027; thus, this compound was identified as jalaric acid.

The retention time of component 4 was 3.72 min, and its pseudo molecular peak $[M\text{-}H]^-$ at the first-stage MS level was m/z 303.21755, which fits the molecular formula $C_{16}H_{32}O_5$. The characteristic fragment ions of this component at the second-stage MS level were observed at m/z 285.20700, 267.19672, 201.11377, 171.10243, and 127.11254. Thus, this compound was identified as aleuritic acid.

According to Ref. [42], these characteristic components prove that the light-red area contains lac dye. The XRD analysis showed that the felsobanyaite was composed of potassium aluminum sulfate dodecahydrate [$KAlSO_4 \cdot 12H_2O$], which is a crystal formed by the processing and refinement of alunite. The presence of K, Al, Na, S, O, and C also indicated that the lac in the mural surface was prepared as a lake pigment by combining water-soluble lac with alkaline potassium alum [$KAlSO_4 \cdot 12H_2O$] [43, 44]. However, lac dye only produces a very weak luminescence when irradiated with 365 nm light in the laboratory setting. The intense pink coloration in the mural could arise from the influence of gypsum in the lower layers and different concentrations of Al^{3+} [45], but further research is necessary to confirm this supposition. Our extensive investigation of the mural revealed that all parts showing salmon luminescence contain lac.

In summary, the light-red areas are composed of a top layer consisting of lac dye, a second layer consisting of gypsum, clinochlore, and quartz (a white clay-mineral mixture), and a third layer consisting of litharge.

Charcoal-gray areas

Many parts of the mural show graying of the pigment layer. A representative example is the oval halo behind the prince's head in Scene 2 (Fig. 3-d[6]). The charcoal-gray areas are shown in black–jade green in the IRRFC image (Fig. 4-d[6]). These areas also emit green luminescence in the 365 nm-excited UVL image (Fig. 6 -d[6]). Based on pDM observations of the gray-colored area, a layer of white material covers a black pigment layer, which explains its gray appearance (Fig. 7-a[6]). The pXRF analysis indicates that this area has a high As content, as well as small amounts of Hg, Fe, and Ca (Fig. 7-b[6]). Microscopic observations of a cross-sectional sample indicated that this area consists of a 13.9 μm-thick white pigment layer (layer 1), a 14.0 μm-thick deep-red pigment layer that also contains a small amount of orange particles (layer 2), and a 33.0 μm-thick olive-green pigment layer (layer 3) (Fig. 8-e[6]). The SEM-EDS analysis showed that the second layer contains Ca, Hg, Si, O, K, Fe, C, Al, Mg, and As and the third layer contains Cl, Ca, Si, Mg, As, Al, O, Fe, C, and S (Fig. 9-c). The XRD analysis of a microsample obtained from the gray area showed quartz [SiO_2], azurite [$(Cu_3CO_3)_2(OH)_2$], gypsum [$CaSO_4 \cdot 2H_2O$], dickite [$Al_2Si_2O_5(OH)_4$], and arsenolite [As_4O_6] phases (Fig. 10-f). The presence of azurite is most likely due to the blue pigments from the prince's hair band, which were introduced during the sampling process. The primary pigments of the gray-colored areas are quartz, gypsum, dickite, and arsenolite.

In summary, the white substance in the charcoal gray area could be arsenolite, which is formed by the oxidation of arsenic sulfide or hydrolysis of arsenic chloride. The base layer of the gray area contains high concentrations of Cl, as well as As and S, which may promote oxidation reactions. Furthermore, Cave 245 had not been sealed for a long time, which resulted in its exposure to sunlight and severe fire damage. Therefore, long periods of illumination by sunlight and high temperatures may have contributed to the oxidative degradation and color changes of sulfidic pigments in the mural [46]. This phenomenon has been reported in the literature. For example, the oxidation of orpiment (As_2S_3, golden yellow) converts it to arsenic oxide (As_2O_3, gray or white) and the oxidation of realgar (a-As_4S_4, orange–red) converts it to

pararealgar (b-As_4S_4, yellow) and then to arsenic oxide [47]. Arsenolite is a dimorph of As_2O_3. Therefore, we deduced that the gray layer was originally composed of a mixture of realgar [a-As_4S_4] and pararealgar [b-As_4S_4] and that arsenolite is an intermediate product of their oxidation processes. The green luminescence in the UVL image was most likely produced by arsenic oxides. The red pigment in the second layer of the cross-sectional sample is cinnabar, which was introduced through contact with the red pigment on the prince's hair band during the sampling process. The olive-green minerals in the third layer are rather interesting, as they may have been formed by the coprecipitation of soluble arsenates (derived from arsenite) with divalent or trivalent cations (e.g., Fe^{2+}/Fe^{3+}, Ca^{2+}, Mg^{2+}, and Al^{3+}) [48]. According to the pXRF analysis, the third layer contains large amounts of Mg, As, Fe, Al, Mn, Si, K, and O, all of which seem to be associated with goethite. However, no signals of a goethite phase were detected in the XRD analysis; instead, the detected mineral phase was more similar to clinochlore [49, 50]. We believe that the failure of the XRD analysis to detect significant clinochlore and Fe_2O_3 phases in the microsample could be attributed to the low concentrations of these phases or pigment mixing, resulting in the obstruction of their signals by background noise or intense reflections from other substrates. The silicates of Fe, K, Mg, and Al are also known to be green in color. Therefore, the olive-green minerals may have originated from clinochlore. We are inclined to believe that clinochlore (formed by the alteration of arsenate and Fe–Mg minerals) was mixed with quartz and dickite in the sandy base layer. The preparatory layer is gypsum, which is covered by realgar.

Brown areas

Inspection of the brown parts of the mural indicated that they consisted of three hues: black–brown, maroon, and red–brown. The black–brown parts are located on human clothes and mountains. Many parts of the mural are colored maroon, including the mountains, skin and clothes of the human characters, and area with holy lights behind the human characters' heads. The red–brown parts are located in the background. As the color and appearance of the black–brown and maroon parts are very similar, delineating their color boundaries in the VISR image (Fig. 3-d[7, 8]) is difficult. However, the IRRFC image shows a small difference in the IR reflectance of these color-areas. In the IRRFC image, the black–brown parts are shown in olive–ochre (Fig. 4-d[7]), while the maroon parts are shown in jade green (Fig. 4-d[8]). In the 365 nm-excited UVL image, the dark-brown area has a weak salmon luminescence similar to that of the light-red area (Fig. 6-d[7, 8]) (full-scene multispectral image A1 in Supplementary Material 1). Microsamples were obtained from damaged parts of the mural in Scene 2 (i.e., the black edges of the mountain range and the dark-brown pigment layer on the edges of the human characters' clothes). Extensive pXRF investigations were also performed on the red–brown area.

Black–brown area

Based on the pDM observations, the black–brown area has a dark-brown pigment layer covered by a layer of black–gray matter (Fig. 7-a[7]). The pXRF analysis shows that the black–brown area contains high concentrations of Fe and As, as well as Ca (Fig. 7-b[7]). Based on microscopic observations of the cross-sectional samples, a 5.8 μm-thick black–gray layer covers 21.6 and 22.0 μm-thick layers of pigment mixtures consisting of yellow and red particles (Fig. 8-f[7]). According to the SEM-EDS analysis, the red–

yellow pigment mixture (layer 2) contains Si, Ca, Fe, Mn, O, Al, As, Mg, Ca, and K (Fig. 9-d). The XRD analysis of the microsample revealed the presence of quartz [SiO_2], carminite [$PbFe_2(AsO_4)_2(OH)_2$] [51], clinochlore [$Mg_5Al(AlSi_3)O_{10}(OH)_8$], cinnabar [HgS], illite [$(K,H_3O)(Al,Mg,Fe)_2(Si,Al)_4O_{10}\ (OH)_2{\cdot}(H_2O)$], and calcite [$CaCO_3$] phases (Fig. 10-g).

The discovery of carminite (a Pb–Fe hydroxyarsenate belonging to the orthorhombic crystal class) in the black–brown area was somewhat unexpected, as it is a rare secondary mineral. The optical appearance of carminite is generally described as carmine or reddish yellow [52, 53]. Indeed, the use of carminite as a pigment would be a very interesting discovery for the technological history of China. Although mimetite, an arsenite, is well known to be used as a paint in the Dazu Rock Carvings in China [54], reports on the direct use of carminite as a mural paint are rare. Carminite is most likely a product of sulfide and arsenide oxidation [55]. Based on tests conducted by the National Museum of American History on pure carminite samples from Mapimi (Mexico), the theoretical composition of the accepted formula of carminite includes PbO, CaO, MgO, FeO, Fe_2O_3, Al_2O_3, As_2O_5, P_2O_5, and water [56]. Fe and As were detected in our XRF analyses, while As, Fe, O, Al, Mg, and Ca were detected in the mixed red–yellow pigment layer by SEM-EDS analysis. These results are consistent with the elemental composition of carminite. As Cave 254 has suffered from severe fire damage and changes in climate, temperature, and humidity, these factors may have rendered the S-containing compounds in a reductive state, thereby increasing their susceptibility to oxidation. This state resulted in the formation of Hg-As oxides or hydroxides and sulfate minerals. Because carminite is an O-containing salt, it is likely to be an intermediate product of cinnabar and realgar oxidation. If this hypothesis is correct, the red–yellow mixture should consist of cinnabar (red), carminite (red), realgar (As_4S_4), and pararealgar (b-As_4S_4) (yellow) [57]. The red and yellow colorations most likely originated from cinnabar and realgar (which was originally orange), respectively. Owing to their crystalline properties, these pigments are incompatible with each other in a painting. The cinnabar was most likely painted on top of a layer of realgar; however, as the crystal grains of these pigments have different specific gravities, the pigments may have eventually mixed with each other. The black–gray matter on the surface could be the final product of arsenic sulfide oxidation, which indicates that As ions migrated through the pigment layers during mural degradation. These findings also imply that this process began from the pigment surface. The preparatory layer is a white clay-mineral pigment mainly consisting of quartz and calcite, which also contains clinochlore and illite.

Maroon and red–brown areas

Based on our extensive pXRF investigations, we discovered that the red–brown area contains high concentrations of Pb and Fe. In the IRRFC images, the red–brown area appears dark yellow–green. As mentioned earlier, the red–black background consists mainly of red lead and litharge.

A detailed investigation was conducted on the maroon areas. The pDM observations show that a layer of pink matter covers another layer of maroon pigment (Fig. 7-a[8]). The pXRF analysis shows that the maroon areas contain high concentrations of Fe, Pb, and Ca (Fig. 7-b[8]). Cross-sectional microscopy indicated that the maroon areas are composed of a total of five pigment layers: a 15.3 μm-thick maroon

layer (layer 1), a 49.3 μm-thick white–maroon mixture (layer 2), a 15.2 μm-thick dark-gray layer (layer 3), a 34.9 μm-thick white–orange mixture (layer 4), and a 16.3 μm-thick orange–red mixture (layer 5) (Fig. 8-g[8]). The SEM-EDS analysis showed that the second layer contains Cl, Ca, Si, Mg, O, Al, Fe, and C; the third layer contains Cl, Ca, Si, As, Mg, O, Pb, and Al; and the fourth layer contains Cl, Ca, Si, Mg, O, Fe, Al, C, and S (Fig. 9-e). According to the XRD analysis of microsamples taken from the same positions, the dark-brown areas contain quartz [SiO_2], carminite [$PbFe_2(AsO_4)_2(OH)_2$], microcline [$(Na,K)AlSi_3O_8$], illite [$(K,H_3O)(Al,Mg,Fe)_2(Si,Al)_4O_{10}$ $(OH)_2{\cdot}(H_2O)$], and calcite [$CaCO_3$] phases. The signals of the carminite, microcline, and quartz peaks are especially strong (Fig. 10-h). Given the stratigraphic complexity of these pigment layers, MLRS was used to analyze the maroon samples. Based on Raman fingerprinting, the white particles contain Lead chloride ($PbCl_2$), while the orange–red particles contain red lead (Pb_3O_4) (Fig. 12). Combining these results with those of the EDS analysis revealed that these components came from the third and fourth layers.

The pigments in the inspected maroon-colored points show a weak luminescence that is similar to that of the light-red and deep red areas. Therefore, the first layer is likely lac dye. This layer is partially mixed with the second layer, which is a calcite-dominated clay-mineral preparatory layer, the purpose of which is to enhance the hue of the lac dye and prevent mixing with the underlying pigment layers. The third layer may have been formed by the oxidation of S, As, and Pb due to their contact with the aforementioned mixture. If we consider the results of the elemental analysis, the elements and colors of the mixing layer between the fourth (white) and fifth (orange–red) layers are similar to those of carminite. Therefore, the products of sulfide and arsenide oxidation could be present in these layers, i.e., the oxidation products of realgar (As_4S_4) and its altered intermediate, pararealgar (b-As_4S_4). Owing to the migration of As ions between the third, fourth, and fifth layers, these ions form an oxide with Pb ions from the third layer, resulting in the formation of a dark-gray layer. Thus, the initial pigment layer in the maroon areas, from top to bottom, may consist of only four pigments layer, namely lac dye, calcite, realgar and red lead. Lead chloride may be used as an extender for realgar.

Deep-red areas

The deep-red and brown areas have a similar color and appearance, and the former is mainly located at the edges of the mountains in the mural (Fig. 3-e[9]). In the IRRFC image, the deep-red areas are orange–brown in color (Fig. 4-e[9]). In the 365 nm-excited UVL image, the deep-red areas have a salmon luminescence that is identical to that of the light-red areas (Fig. 6-e[9]). The pDM observations of a damaged part of the mural reveal a layer of orange–red pigment covering a soil base, as well as a layer of deep-red pigments (Fig. 7-a[9]). The pXRF analysis shows that this region contains high concentrations of Pb and Hg, as well as some Fe (Fig. 7-b[9]). The cross-sectional microscopic images show that the deep-red areas consist of four stacked pigment layers: a 5.2 μm-thick deep-red layer (layer 1), 22.1 μm-thick red layer (layer 2), 21.2 μm-thick orange–yellow layer (layer 3), and 10.1 μm-thick soil-yellow layer (layer 4) (Fig. 8-h). The SEM-EDS analysis shows that the second layer contains a high concentration of Hg, as well as Si, O, Al, As, and C. The third layer has a high Pb content, as well as some O and C (Fig. 9-f).

In the XRD analysis of microsamples from the deep-red area, quartz [SiO_2], carminite [$PbFe_2(AsO_4)_2(OH)_2$], litharge [PbO], cinnabar [HgS], and calcite [$CaCO_3$] phases were detected (Fig. 10-i).

Based on the results above, we can deduce that the pigment layers of the deep-red area contain lac (layer 1), cinnabar (layer 2), and litharge (layer 3). The preparatory layer was made of calcite.

Stratigraphy of the pigment layers

When painting a mural, the layering or mixing of pigments is often necessary to create a desired color or effect. Although the concept of “chemistry” had not been formalized in ancient China, the stratigraphy of the pigment layers revealed that the ancient artists of China understood the concept of chemical compatibility, specifically that some pigments can be chemically compatible or incompatible with each other. In our analyses, we found that the mineral pigments in the mural include azurite, atacamite, Red lead, litharge, cinnabar, gypsum, talc, calcite, and organic dyes, such as lac (Fig. 13).

First, gypsum and calcite were used to create the preparatory layer. However, these white pigments are not used in all areas where the color-pigment layer is in contact with the base layer. Instead, their usage depends on the refractive characteristics of the crystal grains of the color-pigment. They are also used to separate pigment layers that are chemically incompatible with each other. This approach allows the artist to enhance the pigment color while keeping incompatible pigments isolated from each other. For example, gypsum was used below azurite (a Cu-based pigment) to separate it from the alkaline soil in the base layer [58], thus preventing the pigment color from changing owing to reactions with the alkaline soil. Using gypsum as a preparatory layer could also flatten the base layer and enhance the color of the azurite pigment. Gypsum was further used as a preparatory layer when realgar is in contact with the base. In areas where the lac dye comes into contact with litharge, gypsum was used to separate the pigment layers, lighten the redness of the lac dye, and prevent the Pd-based pigment from darkening due to moisture.

Calcite is even more chemically stable and, thus, has better refractive properties than gypsum owing to its crystalline nature. When used as a barrier layer, calcite prevents chemical reactions between chemically incompatible pigments while allowing their colors to mix. In the mural, calcite was used as a barrier layer between the base layer and realgar, between lac and realgar, and between litharge and the base layer. Talc, which has a smooth texture, can be applied with gypsum to enhance the adhesion of the preparatory layer to the soil base. Talc was used to create the surface of the pagoda in Scene 5, giving the pagoda a luster that resembles white jade.

Second, pigment incompatibilities will accelerate their oxidation and color change. Cu-based pigments, such as azurite and atacamite, were never layered with Pb-based pigments, such as red lead and litharge, or As-based pigments, such as realgar, to avoid this issue. Moreover, no contact between realgar and red lead or between cinnabar and red lead was observed. Despite these precautions, however, the pigments in the mural still showed varying degrees of color change and fading. These changes are known to be very complex, as they are driven by a multitude of intrinsic (pigment properties) and extrinsic (the surrounding

environment and microbes) factors. The international literature includes a large body of research on pigment compatibility [59], which has proven to be invaluable for determining pigment compatibilities.

Pigment-painted areas and digital reconstruction

By projecting the pigment analysis results to pigment features in the multispectral images, we can determine the distribution of each pigment in the mural (Fig. 14-[a–j]). The HSB values of each pigment were determined using the VISR images of newly purchased pigment samples (Fig. 14-k). These values were subsequently used to digitally reconstruct the original colors of the mural. In the digital reconstruction, the ideal colors of the pigments were simulated under normal conditions (Fig. 15). Based on the stratigraphy of the painted layers, the painting process was likely to involve 12 steps: (1) drawing of structural lines, (2) coloring with litharge, (3) coloring with red lead, (4) laying of the gypsum base, (5) coloring with azurite and atacamite, (6) coloring with realgar, (7) laying of the calcite barrier, (8) coloring with realgar, (9) coloring with cinnabar, (10) coloring with lac dye, (11) inking of lines, and (12) brightening of highlights (such as white areas on human bodies, organs, clothes, and decorations).

The coloring of human bodies in the mural was performed using a technique called the “convex-and-concave method” (*aotufa*), where gradual changes in color are used to create a sense of three dimensionality. This technique was especially popular during the Northern Wei Dynasty. It is performed by using a deeper color on the inner edge of a contour and then gradually transitioning to a lighter color toward the outer edge, causing limbs to appear more 3D-like. Prominent parts of the human characters’ face, such as the forehead, eyebrows, eyes, bridge of the nose, chin, and middle of the face, are highlighted using white paint. This style of painting proves that the introduction of Indian Buddhist art to China around the 4th century CE had a significant influence on early murals in the Mogao Grottoes. This technique continued to be used in the murals of the Mogao Grottoes until the end of the Tang Dynasty (618–907 CE), at which point a decorative style came to prominence.

Conclusion

In this study, a Northern Wei Dynasty mural in the Mogao Caves was extensively and objectively analyzed to create a digital reconstruction that provides accurate information on its pigment types, painting patterns, and original colors. The relationship between painting processes and pigment degradation (color change and fading) was also described. Differences in pigment origin and size or the selection of binders may affect the final color and appearance of the pigments. Furthermore, simulating the personal style and habits of the artist is quite challenging. These factors render a perfect recreation of the original appearance of ancient murals all but impossible. Nonetheless, because the virtual reconstruction conducted in this study is an objective manifestation of our analytical results, that the aesthetic and artistic value of the mural will be misrepresented owing to subjective reasons is unlikely. This reconstruction may serve as a reference for the study of contemporary murals in other historical sites.

Because of technical limitations, the exact identity of some color-changed pigments and the cause of these color changes require further study. In our future work, we will seek to improve the analytical

methods and approaches used for our virtual reconstruction. We will also employ advanced technologies, such as neural network and machine learning, to recreate the process by which the mural degraded from its original appearance to its current state.

Abbreviations

MSI
Multispectral imaging
VISR
Visible-reflected imaging
IRR
Infrared-reflected imaging
IRRFC
Infrared-reflected false color imaging
UVL
Ultraviolet luminescence imaging
UVR
Ultraviolet-reflected imaging
UVRFC
Ultraviolet-reflected false color imaging
VIL
Visible light-induced infrared luminescence
VIVL
Visible light-induced visible luminescence
pXRF
Portable X-ray fluorescence analyzer
SEM/EDX
Scanning electron microscopy/energy dispersive X-ray spectroscopy
LC/MS
Liquid chromatography/mass spectrometry
pDM
Portable digital microscope
MLRS
Mini laser Raman spectroscopy
UNESCO
United Nations Educational, Scientific and Cultural Organization

Declarations

Availability of data and materials

All of the data that were generated or analyzed during the study period are included in this paper.

Competing Interests

The authors declare no conflict of interest in relation to this publication.

Funding

This study was supported by the National Social Science Foundation of China (Grant Nos. 19EA195), Natural Science Foundation of Gansu Province (Grant No. 20JR5RA055), National Key Research and Development Project of China (Grant No. 2019YFC1520701), Gansu Province Youth Science and Technology Fund (Grant No. 21JR7RA758), and the Science and Technology Project of Gansu Province (Grant No. 21JR7RA759).

Author contributions

CBL performed the multispectral image analysis, microscopic investigation, and digital reconstruction of the mural and wrote the first draft of this paper. SBM, SML conceptualized the main research ideas of this work and guided the direction of this study. YZR provided guidance for the pigment analysis. SZW performed the SEM/EDX analyses on the pigment samples. ZJL performed the LC/MS analyses on the pigment samples. SBW performed the XRD analyses on the pigment samples. WZ performed the MLRS analyses on the pigment samples. YYP performed the in situ pXRF analysis of the mural. All of the authors read and approved the final manuscript.

Acknowledgements

This research received strong support and direction from Professor Wang Xudong of the Palace Museum of China, to whom we are very grateful.

Author information

CBL, associate researcher at the Conservation Institute of Dunhuang Research Academy (Gansu, China). His main research interests lie in the conservation and research of ancient murals.

References

1. Chen H, Chen Q. The digital interpretation and film creation of the picture of Prince Sattva Sacrifices Himself to the Starving Tigress in Cave 254 of Mogao Grottoes. Dunhuang Research. 2014;6:55–60.
2. Martin, AE. Bodily transfer and sacrificial gestures: rethinking the Hungry Tigress Jataka in Mogao Cave 254 [thesis on the Internet]. Utah, USA: Department of Art and Art History, University of Utah. 2014.
3. Pei S, He Y. Study on the importance of protecting the original artistic value of the cultural heritage of the Mogao Grottoes. In: Proceedings of the 4th International Conference on Art Studies: Science,

Experience, Education (ICASSEE 2020): conference proceedings. 2020 Aug 27–28. p. 264-8.

4. Yu S, Wu J, Wang J. Acquisition and processing of the photographic images of the 3D faces inside the narrow caves of the Mogao Grottoes—taking the digitization of the Mogao Cave 254 as an example. Dunhuang Research. 2012;6:108–12.
5. Peitroni E, Ferdani D. Virtual restoration and virtual reconstruction in cultural heritage: terminology, methodologies, visual representation techniques and cognitive models. Information. 2021;12(4):167.
6. Costume and Makeup [Internet]. Dunhuang Academy; 2020 [accessed 2022.3.8]. Available from public.dha.ac.cn/zhuanti/slmz/sec5/section5-1.htm
7. Aswatha SM, Mukherjee J, Bhowmick P. An integrated repainting system for digital restoration of Vijayanagara murals. Int J Image Graph. 2016;16(1):1650005.
8. Wang H-L, Han P-H, Chen Y-M, Chen K-W, Lin X, Lee M-S, et al. Dunhuang Mural restoration using deep learning. In: SA '18: SIGGRAPH Asia 2018: technical brief. 2018 Dec 4–7; Tokyo, Japan. p. 1–4.
9. Stenger J, Khandekar N, Raskar R, Cuellar S, Mohan A, Gschwind RJ. Conservation of a room: a treatment proposal for Mark Rothko's Harvard Murals. Stud Conserv. 2016;61(6):348–61.
10. Wei B, Liu Y, Pan Y. Using hybrid knowledge engineering and image processing in color virtual restoration of ancient murals. IEEE Trans Knowl Data Eng. 2003;15(5):1338–43.
11. Schönlieb C-B. Unveiling the Invisible: mathematical approaches for virtual image restoration in the arts. In: Bridges 2020: Mathematics, Art, Music, Architecture, Education, Culture: conference Proceedings. 2020 Aug 1–5. p. 9–10.
12. Blažek J, Zitová B, Beneš M, Hradilová J. Fresco restoration: Digital image processing approach. In: 17th European Signal Processing Conference (EUSIPCO 2009): conference proceedings. 2009 Aug 24–28; Glasgow, UK. p. 1210-14.
13. Original materials and techniques. In: Agnew N, Wong L, editors. The conservation of Cave 85 at the Mogao Grottoes, Dunhuang. USA: Getty Publications; 2013. p. 155–89.
14. Schilling MR, Mazurek J, Carson D, Bomin S, Yuquan F, Zanfeng M. Analytical research in Cave 85. In: Agnew N, editor. Conservation of ancient sites on the silk road: Proceedings of the Second International Conference on the Conservation of Grotto Sites. USA: Getty Publications; 2010. p. 438 – 64.
15. Ogura D, Nakata Y, Hokoi S, Takabayashi H, Okada K, Bomin S, et al. Influence of light environment on deterioration of mural paintings in Mogao Cave 285, Dunhuang. AIP Conference Proceedings 2170. 2019:020013.
16. Guo Q, Staff RA, Lu C, Cheng L, Dee M, Chen Y, et al. A new approach to the chronology of caves 268/272/275 in the Dunhuang Mogao grottoes: combining radiocarbon dates and archaeological information within a Bayesian statistical framework. Radiocarbon. 2018;60(2):667–79.
17. Xu L, Zhou G, Li Y. Report on the analysis by X-ray diffraction of inorganic pigments used in murals and color sculptures in Mogao Grottoes. Dunhuang Research. 1983:187–97.

18. Li ZX. Pigment analysis on Tang Dynasty murals at the Mogao grottoes. Dunhuang Research. 1993;1:108–17.
19. Nöller R. Cinnabar reviewed: characterization of the red pigment and its reactions. Stud Conserv. 2015;60(2):79–87.
20. Vermeulen M, Sanyova J, Janssens K, Nuyts G, De Meyer S, De Wael K. The darkening of copper-or lead-based pigments explained by a structural modification of natural orpiment: a spectroscopic and electrochemical study. J Anal At Spectrom. 2017;32(7):1331–41.
21. Aze S, Vallet J-M, Baronnet A, Grauby O. The fading of miniumite pigment in wall paintings: tracking the physico-chemical transformations by means of complementary micro-analysis techniques. Eur J Mineral. 2006;18(6):835–43.
22. Wang W, Ma Y, Ma X, Wu F, Ma X, An L, et al. Diversity and seasonal dynamics of airborne bacteria in the Mogao Grottoes, Dunhuang, China. Aerobiologia. 2012;28(1):27–38.
23. Imperi F, Caneva G, Cancellieri L, Ricci, MA, Sodo, A, Visca P. The bacterial aetiology of rosy discoloration of ancient wall paintings. Environ. Microbiol. 2007;9(11):2894–902.
24. Vermeulen M, Janssens K, Sanyova J, Rahemi V, McGlinchey C, De Wael K. Assessing the stability of arsenic sulfide pigments and influence of the binder media on their degradation by means of spectroscopic and electrochemical techniques. Microchem J. 2018;138:82–91.
25. Piqué F, Verri G. UV-Induced Fluorescence Photography. In: Organic materials in wall paintings. USA: Getty Conservation Institute; 2015.18–20
26. Pelagotti A, Del Mastio A, De Rosa A, Piva A. Multispectral imaging of paintings. IEEE Signal Process Mag. 2008;25(4):27–36.
27. Wilson M, France F, Bolser C. Multispectral imaging for scientific analysis and preservation of cultural heritage materials. Archiving Conference. 2018:147 – 50.
28. Cosentino A. Practical notes on ultraviolet technical photography for art examination. Conservar Património. 2015;21:53–62.
29. Verri G, Saunders D. Xenon flash for reflectance and luminescence (multispectral) imaging in cultural heritage applications. The British Museum Technical Bulletin. 2014;8:83–92.
30. Verri G. The spatially resolved characterisation of Egyptian blue, Han blue and Han purple by photo-induced luminescence digital imaging. Anal Bioanal Chem. 2009;394(4):1011–21.
31. Dyer J, Tamburini D, O'Connell ER, Harrison A. A multispectral imaging approach integrated into the study of late antique textiles from Egypt. PLOS One. 2018;13(10):e0204699.
32. Tamburini D, Dyer J. Fibre optic reflectance spectroscopy and multispectral imaging for the non-invasive investigation of Asian colourants in Chinese textiles from Dunhuang (7th-10th century AD). Dyes Pigm. 2019;162:494–511.
33. Colantonio C, Pelosi C, D'Alessandro L, Sottile S, Calabrò G, Melis M. Hypercolorimetric multispectral imaging system for cultural heritage diagnostics: an innovative study for copper painting examination. Eur Phys J Plus. 2018;133(12):526.

34. Cosentino A. Studies. Panoramic, macro and micro multispectral imaging: an affordable system for mapping pigments on artworks. J Conserv Mus Stud. 2015;13(1).
35. Webb EK, Summerour R, Giaccai J. A case study using multiband & hyperspectral imaging for the identification & characterization of materials on archaeological Andean painted textiles. Textile Group Postprints. 2014:24.
36. Dyer J, Verri G, Cupitt J. Multispectral imaging in reflectance and photo-induced luminscence modes: a user manual. The British Museum; 2013.
37. Cosentino A. Identification of pigments by multispectral imaging; a flowchart method. Heritage Sci. 2014;2(1).
38. Caggiani MC, Cosentino A, Mangone A. Pigments Checker version 3.0, a handy set for conservation scientists: a free online Raman spectra database. Microchem J. 2016;129:123–32.
39. de la Rie, E. R. Fluorescence of paint and varnish layers (part 1). Stud. Conserv. 1982;27(1):1–7.
40. Chai B-L, Su B-M, Zhang W-Y, Wang X-W, Li L-Z. Standard multispectral image database for paint materials used in the Dunhuang murals. Spectrosc Spectral Anal.. 2017;37(10):3289.
41. Smith GD, Clark RJ. Note on lead(II) oxide in mediaeval frescoes from the monastery of San Baudelio, Spain. Appl Spectros. 2002;56(6):804–6.
42. Tamburini D, Dyer J, Bonaduce I. The characterisation of shellac resin by flow injection and liquid chromatography coupled with electrospray ionisation and mass spectrometry. Sci. Rep. 2017;7(1):14784.
43. Clementi C, Doherty B, Gentili PL, Miliani C, Romani A, Brunetti, BG, et al. Vibrational and electronic properties of painting lakes. Appl Phys A. 2008;92(1):25–33.
44. Tamburini, D. Investigating Asian colourants in Chinese textiles from Dunhuang (7th-10th century AD) by high performance liquid chromatography tandem mass spectrometry–towards the creation of a mass spectra database. Dyes Pigm. 2019;163:454–74.
45. Nabais P, Melo MJ, Lopes JA, Vieira M, Castro R, Romani A. Organic colorants based on lac dye and brazilwood as markers for a chronology and geography of medieval scriptoria: a chemometrics approach. Heritage Sci. 2021;9(1).
46. Vermeulen M, Nuyts G, Sanyova J, Vila A, Buti D, Suuronen, J-P, et al. Visualization of As(III) and As(V) distributions in degraded paint micro-samples from Baroque-and Rococo-era paintings. J Anal At Spectrom. 2016;31(9):1913–21.
47. Vermeulen M, Sanyova J, Janssens K, Nuyts G, De Meyer S, De Wael K. The darkening of copper-or lead-based pigments explained by a structural modification of natural orpiment: a spectroscopic and electrochemical study. J Anal At Spectrom. 2017;32(7):1331–41.
48. Vanmeert F, de Keyser N, van Loon A, Klaassen L, Noble P, Janssens K. Transmission and reflection mode macroscopic X-ray powder diffraction imaging for the noninvasive visualization of paint degradation in still life paintings by Jan Davidsz. de Heem. Anal Chem. 2019;91(11):7153–61.

49. Gebremariam, KF, Kvittingen L, Banica F-G. Physico-chemical characterization of pigments and binders of murals in a church in Ethiopia. Archaeometry. 2016;58(2):271–83.
50. Lama E, Prieto-Taboada N, Etxebarria I, Bermejo J, Castro K, Arana G, et al. Spectroscopic characterization of xx century mural paintings of punta begoña's galleries under conservation works. Microchem J. 2021;168:106423.
51. Rosenzweig A, Finney JJ. The unit cell of carminite. Am Mineral. 1959;44:663–5.
52. Mazzoleni P, Barone G, Raneri S, Aquilia E, Bersani D, Cirrincione, R. Application of micro-Raman spectroscopy for the identification of unclassified minerals preserved in old museum collections. Plinius. 2016;42:112–24
53. Yi L, Laren L. Preliminary study of the characteristics and genesis of arsenate minerals in the oxidized zone of the Debao skarn-type Cu-Sn ore deposit in Guangxi. 1991;4(2):187–94.
54. Wang LQ, Ma YN, Zhang YX, Zhao X, He QJ, Guo JY, et al. Pigment identification of Sleeping Buddha at World Cultural Heritage Dazu Rock Carvings with mu-Raman spectroscopy and related research. Spectrosc Spectral Anal. 2020;40(10):3199–204.
55. Taylor MR, Bevan DJM, Pring A. The crystal structure of carminite: refinement and bond valence calculations. Mineral Mag. 1996;60(402):805–11.
56. Foshag WF. Carminite and associated minerals from Mapimi, Mexico. Am Mineral. 1937;22:479–84.
57. Corbeil MC, Helwig K. An occurrence of pararealgar as an original or altered artists' pigment. Stud Conserv. 1995;40(2):133–8.
58. Zhang Y, Wang J, Liu H. Integrated analysis of pigments on murals and sculptures in Mogao grottoes. Anal Lett. 2015;48(15):2400–13.
59. Coccato A, Moens L, Vandenabeele P. On the stability of mediaeval inorganic pigments: a literature review of the effect of climate, material selection, biological activity, analysis and conservation treatments. Heritage Sci. 2017;5(1).

Figures

Figure 1

Current condition of the "Prince Sattva" mural on the south wall of Cave 254: (a) Cave section and floor plan, (b) cave scene, and (c) Prince Sattva.

Figure 2

Multispectral investigation of the mural details.

Figure 3

VISR imaging of the Prince Sattva mural.

Figure 4

IRRFC imaging of the Prince Sattva mural.

Figure 5

UVRFC imaging of the Prince Sattva mural.

Figure 6

UVL imaging of the Prince Sattva mural.

Figure 7

Non-invasive XRF analysis of nine color-areas: (a) Microscopic images of the nine XRF-analyzed areas and (b) the corresponding XRF spectra.

Figure 8

Cross-sectional microscopy of microsamples from nine color-areas.

Figure 9

SEM-EDS analysis of cross-sectional samples taken from nine color-areas: (a) Blue + bean green, (b) light red, (c) charcoal gray, (d) black–brown, (e) maroon, (f) deep red. The SEM-EDS spectrum corresponding to each analyzed point is marked in violet, red, or green.

Figure 10

XRD analysis of pigment samples from nine color-areas.

Figure 11

LC-MS analysis of pigment samples from areas with salmon fluorescence. (a. light red and deep red LC analysis. b. component 1 MS level, c. component 2 MS level, c. component 3 MS level, d. component 4 MS level)

Figure 12

MLRS analysis of the pigment sample from Sampling Location No. 8.

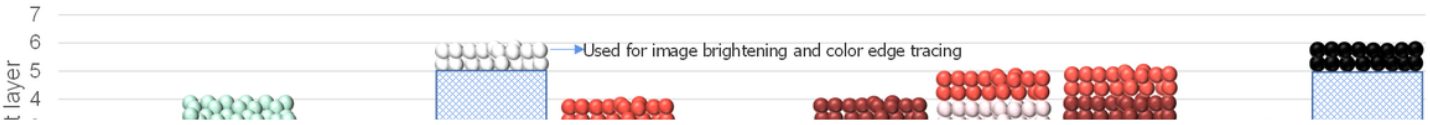

Figure 13

Model of pigment stratigraphy (horizontal axis: current colors of the mural's pigments; vertical axis: pigment layers).

Figure 14

Areas in which each pigment was used and their hue: (a. litharge, b. red lead, c. gypsum, d.azurite, e.atacamite, f.realgar, g.calcite, h.cinnabar, l.lac, j.talc. k.Visible-light palette and HSB values of the pigments used in the mural.)

Figure 15

Digital reconstruction of the Prince Sattva mural.

Supplementary Files

This is a list of supplementary files associated with this preprint. Click to download.

- SupplementaryMaterials.docx